Cooperative Nucleotide Binding to the Human Erythrocyte Sugar Transporter†

Erin K. Cloherty, Kara B. Levine, Christopher Graybill, and Anthony Carruthers*

Department of Biochemistry and Molecular Pharmacology, Lazare Research Building, University of Massachusetts Medical School, 364 Plantation Street, Worcester, Massachusetts 01605

Received March 29, 2002; Revised Manuscript Received July 11, 2002

ABSTRACT: The human erythrocyte glucose transport protein (GluT1) is an adenine nucleotide binding protein. When complexed with cytosolic ATP, GluT1 exhibits increased affinity for the sugar export site ligand cytochalasin B, prolonged substrate occlusion, reduced net sugar import capacity, and diminished reactivity with carboxyl terminal peptide-directed antibodies. The present study examines the kinetics of nucleotide interaction with GluT1. When incorporated into resealed human red blood cell ghosts, (2,3)-trinitrophenyl-adenosine-triphosphate (TNP-ATP) mimics the ability of cytosolic ATP to promote high-affinity 3-O-methylglucose uptake. TNP-ATP fluorescence increases upon interaction with purified human red cell GluT1. TNP-ATP binding to GluT1 is rapid ($t_{1/2} \sim 0.5$ s at 50 μM TNP-ATP), cooperative, and pH-sensitive and is stimulated by ATP and by the exit site ligand cytochalasin B. Dithiothreitol inhibits TNP-ATP binding to GluT1. GluT1 preirradiation with saturating, unlabeled azidoATP enhances subsequent GluT1 photoincorporation of [γ-^{32}P]azidoATP. Reduced pH enhances azidoATP photoincorporation into isolated red cell GluT1 but inhibits ATP modulation of sugar transport in resealed red cell ghosts and in GluT1 proteoliposomes. We propose that cooperative nucleotide binding to reductant-sensitive, oligomeric GluT1 is modulated by a proton-sensitive saltbridge. The effects of ATP on GluT1-mediated sugar transport may be determined by the number of ATP molecules complexed with the transporter.

The facilitated diffusion of sugars across cell membranes is mediated by a family of integral membrane proteins called glucose transporters. Sugar transport in nucleated and anucleate erythrocytes is mediated by the glucose transport protein GluT1[1] (*1*−*4*). Although each GluT1 protein appears to function as a transport pathway, the native form of the glucose transporter in erythrocytes is a GluT1 homotetramer (*5*−*7*). This complex is characterized by cooperative subunit interactions and is subject to allosteric regulation by intracellular ATP (*4*, *7*−*9*).

ATP binding to GluT1 alters the tertiary structure of the GluT1 carboxyl terminus (*8*) and inhibits the release of newly imported sugars from an "occlusion cage" or vestibule formed by cytoplasmic domains of GluT1 (*10*). The functional consequence of these changes is inhibition of GluT1-mediated net sugar uptake (*9*). ATP regulation of GluT1 does not require nucleotide hydrolysis and is competitively inhibited by intracellular AMP or ADP. These nucleotides compete with ATP for binding to the glucose transporter but are unable to mimic the actions of ATP on sugar transport and transporter tertiary structure (*8*, *9*).

Previous studies from this laboratory have demonstrated that GluT1 photolabeling by azidoATP is enhanced by reduced pH (*11*). Paradoxically at low pH where ATP binding to GluT1 is increased, low concentrations of intracellular ATP (<200 μM) modulate sugar transport, but higher concentrations (>1 mM) fail to affect sugar transport in resealed red cell ghosts (*11*). The present study examines the kinetics and pH sensitivity of nucleotide binding to GluT1 and investigates the role of GluT1/ATP interactions in glucose transport regulation by GluT1 reconstitution into proteoliposomes.

MATERIALS AND METHODS

Materials. 8-Azido[γ^{32}P]ATP was purchased from ICN, Costa Mesa, CA. [^{3}H]-2-Deoxy-D-glucose and [^{3}H]-3-O-methylglucose were purchased from Dupont NEN, Wilmington, DE. Gradient SDS PAGE gels were purchased from Owl Scientific, Portsmouth, NH. Nitrocellulose and Immobilon-P were obtained from Fisher Scientific, Pittsburgh, PA. TNP-ATP was obtained from Molecular Probes Inc., OR. All remaining materials were purchased from Sigma unless stated otherwise.

Antisera. A peptide corresponding to GLUT1 residues 480−492 was synthesized by the University of Massachusetts Medical School Peptide Synthesis facility. This peptide was conjugated to keyhole limpet hemocyanin using a kit purchased from Pierce. Rabbit antisera (C-Ab) against this GluT1 peptide were obtained from Animal Pharm Services Inc of Healdsburg, CA.

Solutions. Phosphate-buffered saline (PBS) contained 140 mM NaCl, 10 mM Na_2HPO_4, 3.4 mM KCl, 1.84 mM KH_2-

† This work was supported by NIH Grant DK 36081.

* To whom correspondence should be addressed. Voice: 508 856 5570. FAX: 508 856 6464. E-mail: anthony.carruthers@umassmed.edu.

[1] Abbreviations: GluT1, human erythrocyte glucose transport protein; 2DOG, 2-deoxy-D-glucose; 3MG, 3-*O*-methyl-α,D-glucopyranoside; C-Ab, rabbit polyclonal antiserum raised against a synthetic peptide comprised of GluT1 residues 480−492; CCB, cytochalasin B; CCD, cytochalasin D; EDTA, ethylenediaminetetraacetic acid; HEPES, (N-[2-hydroxyethyl]piperazine-N′-[2-ethanesulfonic acid]); RBC, red blood cell; SDS-PAGE, sodium dodecyl sulfate-polyacrylamide gel electrophoresis; TNP-ATP, 2-(or 3-)trinitrophenyl-adenosine-triphosphate; Tris-HCl, tris(hydroxymethyl)aminomethane.

10.1021/bi0259002 CCC: $22.00
Published on Web 09/26/2002

PO_4 (pH 7.3), and 5 mM EDTA. In some experiments 140 mM KCl was substituted for NaCl in PBS. Lysis buffer consisted of 10 mM Tris-HCl (pH 7.5), and 0.5 mM $MgCl_2$. Tris medium included 50 mM Tris-HCl and 5 mM $MgCl_2$ (pH 7.4). Sample buffer (2X) contained 0.125M Tris-HCl, (pH 6.8), 4% SDS, 20% glycerol, and 50 mM DTT.

Red Cells and Red Cell Ghosts. Human red cells were prepared from whole human blood by washing in saline as described previously (*11*). Red cell ghosts were prepared by hypotonic lysis in lysis buffer at 4 °C and, following resuspension in isotonic KCl−PBS containing molecular species of interest, were resealed by warming to 37 °C for 40 min (*11*).

Purified GluT1. Unsealed, human red cell ghosts were depleted of peripheral membrane proteins and residual cytosolic proteins by a single alkaline wash as described previously (*11*). GluT1 was purified from the remaining integral membrane proteins in the absence of reductant by solubilization in octylglucoside and ion exchange chromatography as described previously (*11*).

Polyacrylamide Gel Electrophoresis. Proteins were resolved on 10% acrylamide gels as described in ref *12*.

Western Blotting. GLUT1was detected by Western blot analysis. Peptides separated by SDS-PAGE were transferred electrophoretically to nitrocellulose membranes, which were subsequently blocked for 1 h in PBS-T (PBS + 0.1% Tween detergent) with 20% Carnation nonfat dry milk. Following three washes of five minutes in PBS-T, membranes were incubated for 1 h in primary antibody. C-Ab was diluted 1:10 000 in 3% nonfat dry milk/PBS-T. Following four wash cycles to remove primary antibody, membranes were exposed for 45 min to secondary antibody (goat anti rabbit IgG -horseradish peroxidase conjugates) diluted 1:5000 in PBS-T containing 3% or 2% nonfat dry milk. Detection of antigen−antibody complexes was achieved by chemiluminescence using Amersham ECL reagents.

Stopped-Flow Fluorescence Measurements. The time-course of TNP-ATP binding to GluT1 was monitored using a Hi-Tech Scientific SF- 61DX2 stopped-flow system. TNP-ATP fluorescence undergoes significant self-quenching at [TNP-ATP] > 40 μM. This results in reduced signal-to-noise and limits the useful working range for [TNP-ATP] to 500 μM. GluT1 (50 μL of a sample containing 20 μg GluT1/mL of saline) was mixed with TNP-ATP (50 μL saline containing 0−5000 μM TNP-ATP) and driven into the light path of the flow cell within 1.5 ms by using a pneumatic drive system. Excitation was at 408 nm, and emission at all wavelengths above 500 nm was collected by use of a photomultiplier. Excitation slit widths of 5 nm were used. A reference photomultiplier was used to monitor fluctuations in the output of the source of excitation and thereby reduce background noise. The flow cell and solution reservoirs were maintained at 20 °C using a temperature-controlled circulating water bath. Data were sampled every 10 μs and, in most experiments, averaged over a time interval of 1 ms. The dead time of the mixing path (1.53 ± 0.03 ms) was confirmed by analysis of the time course of *N*-acetyltryptophanamide (NATA) fluorescence quenching by *N*-bromosuccinamide (NBS) at 20 °C as described previously (*13*). In experiments where H^+, CCB, ATP, or AMP modulation of TNP-ATP binding was measured, GluT1- and TNP-ATP-containing solutions also contained equal concentrations of the test species prior to mixing and injection into the light path.

Glucose Carrier Labeling with 8-Azido[γ-^{32}p]ATP. Labeling was carried out a described previously in ref *11*. A methanolic solution of 8-azido[γ-^{32}P]ATP was dried under nitrogen and resuspended in Tris medium at pH 5.5 or 8.0. GluT1 proteoliposomes were combined with the methanol-free 8-azido[γ-^{32}P]ATP solution (90 μCi ^{32}P; 10 μM final azidoATP concentration; [GluT1] = 1 μg/μL). The suspension was incubated on ice for 30 min to allow equilibrium ATP binding to GLUT1. Samples were placed on ice in separate wells of an ELISA dish, and irradiated for 90 s at 280 nm in a Rayonet Photochemical Reactor. Following UV irradiation (photolabeling), samples (20 μg protein) were resolved on 10% SDS-PAGE gels and transferred electrophoretically to nitrocellulose membranes. Proteins labeled with 8-azido[γ-^{32}P]ATP were visualized by autoradiography and quantitated by densitometry.

3MG Uptake by Red Cells and Red Cell Ghosts. Sugar transport by red cells was as described previously (*11*). In brief, sugar-free cells or resealed erythrocyte ghosts at ice temperature were exposed to five volumes of ice cold KCl−PBS containing [^{3}H]-3-O-methylglucose and variable concentrations of unlabeled 3-O-methylglucose. Uptake was allowed to proceed over intervals of 15 s to 1 min; then 50 volumes (relative to cell volume) of ice-cold stopper solution were added to the cell/ghost suspension. Cells/ghosts were sedimented by centrifugation (14 000*g* for 30 s), washed once in stopper, collected by centrifugation, and extracted in 500 μL of 3% perchloric acid. The acid extract was centrifuged, and duplicate samples of the clear supernatant were counted. Zero-time uptake points were prepared by addition of stopper to cells/ghosts prior to addition of medium containing sugar and radiolabel. Cells/ghosts were immediately processed. Radioactivity associated with cells/ ghosts at zero-time was subtracted from the activity associated with cells/ghosts following the uptake period. All uptakes were normalized to equilibrium uptake where cells/ghosts were exposed to sugar medium at 37 °C for 60 min prior to addition of stopper. Uptake assays were performed using solutions and tubes preequilibrated to 4 °C. In some experiments, cells were preloaded with 50 mM unlabeled 3MG by incubation in 10 volumes 50 mM 3MG for 60 min at 37 °C. Loaded cells were concentrated by centrifugation, and the cell pellet was equilibrated to 4 °C prior to transport determinations.

Reconstituted GluT1-Mediated Sugar Transport. Purified human red cell GluT1 was reconstituted into proteoliposomes by using a detergent dialysis/freeze−thaw procedure as described previously (*11*). The detergent used to solubilize purified GluT1 and exogenous lipids was octylglucoside (48 mM). The exogenous lipids were egg phosphatidylcholine (Type III-E, Sigma Chemicals) and cholesterol. GluT1, phosphatidylcholine, and cholesterol were reconstituted at a ratio (by mass) of 0.1:40:20. A typical reconstitution contained 100 μg GluT1. Net uptake of 3MG at 20 °C by sugar-free GluT1 proteoliposomes from media containing saturating (120 mM) 3MG was monitored by following transport induced volume changes by light scattering as described previously (*14*). In brief, proteoliposomes (5 μL, 0.5 μg GluT1) were injected into a constantly stirred fluorimeter cuvette containing 2 mL 120 mM test sugar in saline. Excitation and emission were both 410 nm with 5

nm slit widths. Initially, proteoliposomes shrink due to osmotic water loss then reswell as sugar is transported into the interior of the proteoliposomes and water follows. Analysis of transport by monitoring light scattering changes assumes that (1) light scattering changes are proportional to proteoliposomal volume, (2) volume changes are rate-limited by sugar transport not by water transport, and (3) volume changes are ideal. While assumptions 1 and 3 are not strictly valid, the errors introduced by these assumptions are within the range of experimental variation (*15*). Uptake of 100 μM [^{3}H]3MG by proteoliposomes was measured at 4 °C at 0, 30, and 60 s and at 1 h by using a centrifugation/wash procedure as described previously for red cells and proteoliposomes (*11*). Uptake at 30 and 60 s was corrected for zero-time uptake and normalized to zero-time-corrected equilibrated proteoliposomal volume measured at 1 h. In experiments where [ATP] or [H^+] were varied, these species were introduced into proteoliposomes during the freeze/thaw steps of reconstitution and were present at the exterior of proteoliposomes throughout the transport procedure.

Data Analysis. Analysis of 8-bit densitometric scans of autoradiograms and immunoblots was carried out using NIH Image 1.62. Curve fitting by nonlinear regression was carried out using the software program Kaleidagraph v 3.51 (Synergy Software, Reading, PA). Fluorescence time course data resolved as single, double, or triple exponentials were analyzed using the following equations, respectively:

$$F = E_0 + E_1(1 - e^{(-k_1 t)}) \quad (1)$$

$$F = E_0 + E_1(1 - e^{(-k_1 t)}) + E_2(1 - e^{(-k_2 t)}) \quad (2)$$

$$F = E_0 + E_1(1 - e^{(-k_1 t)}) + E_2(1 - e^{(-k_2 t)}) + E_3(1 - e^{(-k_3 t)}) \quad (3)$$

where F is fluorescence at time t, E_o is fluorescence at time zero, and k_1, k_2, k_3 are rate constants describing the rate of increase in fluorescence to levels E_1, E_2, and E_3.

Time-course data were also analyzed using a second-order rate equation (*16*) describing the reaction A + B → C where A ≠ B:

$$F = \frac{B_o\left(e^{kt(A_o - B_o)}\frac{A_o}{B_o}\right) - A_o}{\left(e^{kt(A_o - B_o)}\frac{A_o}{B_o}\right) - 1}E_1 + E_o \quad (4)$$

where F is fluorescence at time t, E_o is fluorescence at time zero, k is the second-order rate constant (μM^{-1} s^{-1}) describing the reaction A + B → C, A_o and B_o are starting concentrations of A (TNP-ATP; 2.5−500 μM) and B (GluT1, 0.18 μM), respectively, and E_1 is a constant relating increasing [C] to the increase in fluorescence. If E_1 were set to unity and E_o to zero, this expression would describe the time course of increase in [C].

Simulations of reaction time course were carried out using the software program Berkeley Madonna v 8.01 (University of California, Department of Molecular and Cellular Biology, Berkeley, CA; http://www.berkeleymadonna.com). TNP-ATP (N) binding to GluT1 (G) was simulated by assuming that each transporter is comprised of four subunits (GluT1 proteins), that each subunit contains a nucleotide binding site, that fluorescence is proportional to bound [TNP-ATP], and that binding is consistent with the Adair-Pauling simple sequential interaction model (*17*) (Scheme 1).

Scheme 1

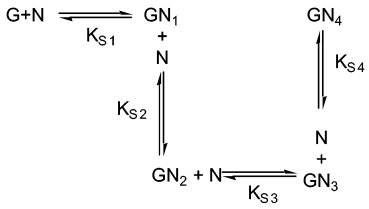

K_S is the intrinsic dissociation constant (k_{-1}/k_1) of an isolated nucleotide binding site and

$$K_{S1} = K_S/4$$

where K_{S1} is the effective dissociation constant of the GN_1 complex (all four sites are equivalent before any nucleotide binds). If the binding of the first nucleotide molecule changes the intrinsic dissociation constants of the vacant sites by the factor a, then $K_{S2} = a2K_S/3$ is the effective dissociation constant. If binding of the second nucleotide molecule changes the intrinsic dissociation constants for the remaining vacant sites by a factor b, then

$$K_{S3} = ab3K_S/2$$

If binding of the third nucleotide molecule changes the intrinsic dissociation constants for the remaining vacant site by a factor c, then

$$K_{S3} = abc4K_S$$

The fraction of glucose transporter that exists as G (uncomplexed with nucleotide), at any given nucleotide concentration [N], is given by

$$\frac{G}{G_T} = \frac{1}{G_o}$$

where

$$G_o = 1 + 4\frac{[N]}{K_S} + 6\frac{[N]^2}{aK_S{}^2} + 4\frac{[N]^3}{a^2bK_S{}^3} + \frac{[N]^4}{a^3b^2cK_S{}^4}$$

where G_T is the concentration of all forms of the glucose transporter.

The fraction of glucose transporter containing a single bound nucleotide is

$$\frac{GN_1}{G_T} = \frac{4\frac{[N]}{K_S}}{G_o} \quad (5)$$

The fraction of glucose transporter containing two bound nucleotides is

$$\frac{GN_2}{G_T} = \frac{6\frac{[N]^2}{aK_S^2}}{G_o} \quad (6)$$

The fraction of glucose transporter containing three bound nucleotides is

$$\frac{GN_3}{G_T} = \frac{4\frac{[N]^3}{a^2\,bK_S^3}}{G_o} \quad (7)$$

The fraction of glucose transporter containing four bound nucleotides is

$$\frac{GN_4}{G_T} = \frac{\frac{[N]^4}{a^3b^2\,cK_S^4}}{G_o} \quad (8)$$

Flows between molecular species were computed as

$$\frac{\partial[GN]}{\partial t} = 4k_1[N][G] - k_{-1}[GN] \quad (9)$$

$$\frac{\partial[GN_2]}{\partial t} = 3k_1[N][GN] - a2k_{-1}[GN_2] \quad (10)$$

$$\frac{\partial[GN_3]}{\partial t} = 2k_1[N][GN_2] - 3abk_{-1}[GN_3] \quad (11)$$

$$\frac{\partial[GN_4]}{\partial t} = k_1[N][GN_3] - 4abck_{-1}[GN_4] \quad (12)$$

This analysis assumes that cooperativity affects only TNP-ATP dissociation from GluT1 (k_{-1}). It is also possible that TNP-ATP association with GluT1 (k_1) is affected by TNP-ATP binding. This was not addressed by the present analysis.

Transport induced light scattering changes in GluT1 proteoliposomes were analyzed using the software package Berkeley Madonna (v 8.0.1; http://www.berkeleymadonna-.com). Each scattering record was normalized to proteoliposomal scattering at zero time. The analysis assumes that (1) a fraction of total proteoliposomal volume is unresponsive to osmotic challenge (dead volume, V_d), (2) a fraction of the remaining proteoliposomes does not incorporate GluT1 (V_{nt}) and is characterized by a surface area A_{nt}, (3) the GluT1-free population are characterized by an osmotic water permeability coefficient of Pf_{nt}, (4) the remaining fraction of proteoliposomes (V_t) is characterized by a surface area A_t and by a distinct osmotic water permeability coefficient Pf_t, (5) the proteoliposomal surface density of transporter in GluT1-containing proteoliposomes is T_d, (6) the osmolality of nontransported species in solution (C_{imp}) is 315 mosmol/L, (7) the extraliposomal concentration of transported species (C) is 120 mmol/L, and (8) sugar transport via reconstituted proteins is characterized by a variant of the fundamental carrier-mediated transport equation (*18*)

$$J_{21} = \frac{K(C_2 - C_1)}{K^2R_{oo} + KR(C_1 + C_2) + R_{ee}C_1C_2} \quad (13)$$

where C_1 and C_2 are concentrations of transported sugar on sides 1 (inside) and 2 (outside of the proteoliposome; K is an intrinsic affinity constant (units of concentration), and R_{oo}, R_{ee}, and R are resistance parameters with units of cm^2 s mol^{-1}. The transport equation normally contains two resistance parameters R_{12} and R_{21} for net exit and uptake but because reconstituted GluT1 has a scrambled orientation, these terms may be grouped as R. R is the reciprocal of V_{max} for net uptake and net exit. R_{ee} is the reciprocal of V_{max} for unidirectional exchange transport (saturating sugar at both sides of the membrane). Because transport is passive, the simplifying assumption $R_{oo} = 2R - R_{ee}$ may be made (*19*). Proteoliposomal diameter (248 ± 15 nm) was determined by dynamic light scattering by using a Precision Detectors PD2000 DLS. Calculations of liposomal isotonic volume and area assume that proteoliposomes are spheres.

Changes in proteoliposomal volume were calculated assuming the following flows:

$$J_{wnt} = Pf_{nt}A_{nt}(Osm_i - Osm_o)$$

water flow into GluT1-free proteoliposomes

$$J_{wt} = Pf_tA_t(Osm_i - Osm_o)$$

water flow into GluT1 proteoliposomes

$$J_{21} = A_t\frac{K(C_2 - C_1)}{K^2R_{oo} + KR(C_1 + C_2) + R_{ee}C_1C_2}$$

sugar flow into GluT1 proteoliposomes

$Osm_o = C_{imp} + C_2$. For sugar transporting proteoliposomes, $Osm_i = (C_{imp} + C_1)/V_t$, while for nontransporting liposomes, $Osm_i = C_{imp}/V_{nt}$. Parameter fitting was carried out by nonlinear regression by simulating time courses by 4th-order Runge Kutta numerical integration. Parameters solved were T_d, R_{oo}, R_{ee}, R, K, Pf_{nt}, Pf_t, V_d, V_{nt}, and V_t. Starting estimates of $T_d{\cdot}R_{oo}$, $T_d{\cdot}R_{ee}$, and $T_d{\cdot}R$ were those exhibited by red cell-resident GluT1 at 20 °C (6.5, 0.7, and 3 ms respectively (*20*)).

RESULTS

Trinitrophenyl-Adenosine Triphosphate Interaction with GluT1. TNP-ATP is an ATP analogue that interacts with the Na,KATPase, the red blood cell Ca/Mg ATPase and with adenylate kinase (*21*−*23*). In human red cells, ATP serves to reduce K_{mapp} and V_{max} for net sugar uptake (*9*). Here, we report that TNP-ATP substitutes for ATP in nucleotide modulation of sugar transport. Comparison of initial rates of cytochalasin B-inhibitable uptake at 100 μM 3MG and 4 °C by nucleotide-free, resealed ghosts (1.9 ± 0.3 μmol L^{-1} min^{-1}; $n = 6$), by resealed ghosts containing 2 mM ATP (9.5 ± 2.0 μmol L^{-1} min^{-1}; $n = 6$) and by resealed ghosts containing 2 mM TNP-ATP (19.3 ± 2.4 μmol L^{-1} min^{-1}; $n = 6$) indicates that ATP and TNP-ATP restore high-affinity transport to red cell ghosts. Cytochalasin B-insensitive transport by ghosts (3.8 ± 0.2 μmol L^{-1} min^{-1}; $n = 6$) is unaffected by the presence of intracellular nucleotide.

TNP-ATP fluorescence (excitation at 408 nm, emission at 540 nm) is increased when TNP-ATP is bound by proteins (*21*). Analysis of TNP-ATP interaction with GluT1 by stop-flow fluorescence reveals that mixing of GluT1 and 50 μM

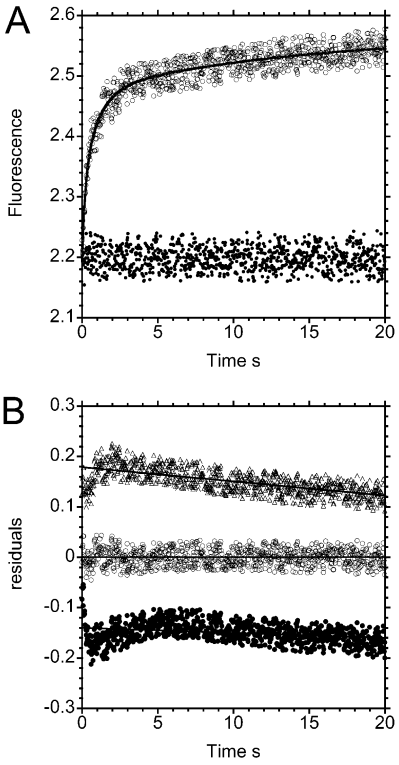

FIGURE 1: Time course of TNP-ATP binding to GluT1 by stop flow fluorescence. (A) At zero-time, 10 μg GluT1 proteoliposomes in 50 μL saline (○) was mixed with 50 μL 100 μM TNP-ATP. The suspension was excited at 408 nm, and emission at wavelengths ≥500 nm was collected. Each data point is the average of four separate measurements collected over an interval of 10 ms. The curve drawn through the data points was computed by nonlinear regression assuming that the increase in fluorescence is described by the Adair Pauling sequential interaction mechanism of Scheme 1. The following constants were obtained: $K_N = 580$ μM, $k_1 = 5.3 \times 10^3$ M^{-1} s^{-1}, $a = 0.85$, $b = 0.1$, $c = 0.01$. Experiments were also made using GluT1-free lipid vesicles (●) formed from total lipids extracted from GluT1 proteoliposomes. (B) The data of Figure 1A were fitted as a single (●) or as two (○) exponential processes (eqs 1 and 2) or as a second-order process (△; eq 4) by nonlinear regression. The residuals are plotted as a function of time. All residuals are centered about 0 on the *y*-axis but, to facilitate inspection, have been displaced by −0.15 for the single-exponential analysis and by +0.15 for the second-order rate law analysis. The resulting constants were obtained: single exponential, $C = 2.293 \pm 0.001\%$, $k_1 = 0.593 \pm 0.019$ s^{-1}, $\Delta E = 0.235 \pm 0.005\%$, $R^2 = 0.825$; two exponentials, $C = 2.214 \pm 0.007\%$, $k_1 = 1.88 \pm 0.11$ s^{-1}, $\Delta E_1 = 0.235 \pm 0.007\%$, $k_2 = 0.129 \pm 0.015$ s^{-1}, $\Delta E_2 = 0.10 \pm 0.003\%$, $R^2 = 0.891$; second-order fit, $B_o = 0.18$ μM, $A_o = 50$ μM, $k = 2.8 \times 10^4$ M^{-1} s^{-1}, $E_o = 2.2$, $E_1 = 1.6$, $R^2 = 0.813$.

TNP-ATP (mixing time = 1.5 ms) produces a rapid increase ($t_{0.5} \sim 0.5$ s) in fluorescence (see Figure 1A). Purified GluT1 forms unsealed proteoliposomes characterized by a random topographical orientation of GluT1 protein (*13*). Because the lipid bilayer is extremely impermeable to ATP (*24*), the delay in achieving steady-state fluorescence is unlikely to result from trans-bilayer diffusion of TNP. Neither is the delay caused by slow equilibration of the interior of leaky proteoliposomes with extraliposomal TNP-ATP. The low proteoliposomal radius ($\lambda = 0.1$ μM as judged by phase contrast microscopy) and relatively high coefficient for self-diffusion of ATP in water ($D = 5 \times 10^{-5}$ cm^2 s^{-1}) suggest an upper limit for the time required for equilibration of extra- and intraliposomal contents of 1 μs ($t_{av} = 0.5$ λ^2/D). Interaction with the hydrophobic lipid bilayer does not account for the increase in TNP-ATP fluorescence upon mixing GluT1 and TNP-ATP because protein-free liposomes formed from lipids extracted from GluT1 proteoliposomes do not produce a rapid increase in fluorescence upon mixing with TNP-ATP (see Figure 1A). The instantaneous ($t_{0.5} = 2$ ms) increase in fluorescence observed upon rapid mixing of TNP-ATP (50 μM) and 10% ethanol in saline suggests that the slower increase in TNP-ATP fluorescence upon mixing with GluT1 results from either (1) the second-order reaction of TNP-ATP with GluT1 or (2) a subsequent GluT1 conformational change promoted upon TNP-ATP binding.

The time course of fluorescence increase upon mixing TNP-ATP and GluT1 at pH 7.4 is quantitatively described by multiple (two or more) first-order reactions. Figure 1 B illustrates how the residuals of a single first-order reaction fit to 50 μM TNP-ATP binding data are not symmetrically distributed about the *x*-axis. A two-component first-order analysis is more successful in describing these data. These findings suggest that TNP-ATP binding to GluT1 is more complex than anticipated—proceeding as multiple first-order reactions in series and/or in parallel—or that binding conditions may require second-order rate analysis.

For the second-order reaction A + B → C, deviations from simple exponential kinetics are expected when [A] ∼ [B]. In the present study, starting [TNP-ATP] (2.5−500 μM) is always much greater than starting [GluT1] (0.18 μM), suggesting that the reaction should be first-order with respect to [TNP-ATP]. Nonlinear regression analysis of the time-course of 50 μM TNP-ATP binding assuming the simple second-order rate law describing the reaction A + B → C, where [A] ≠ [B] (see ref *16*), results in predicted time courses (single exponentials) that deviate significantly from the observed time course (Figure 1B).

If deviations from simple first-order kinetics are not explained by simple second-order reaction conditions, why are the experimental data consistent with multiple first-order reactions? The curve drawn through the time course of Figure 1A represents the predicted time course (a best fit obtained by nonlinear regression) if ligand binding is a cooperative process in which four nucleotides bind successively to the glucose transporter (see Scheme 1). The possibility of cooperative ligand binding kinetics is examined further in the Discussion. However, these data may also be subjected to quantitative analysis in the absence of an assumed ligand binding mechanism. Each binding reaction is comprised of two or more first-order reactions (Figure 1 B). We have subjected each TNP-ATP binding time course at each [TNP-ATP] to two-component first-order reaction analysis to obtain k_{obs1} and k_{obs2} (fast and slow first-order rate constants) and E_1 and E_2 (equilibrium fluorescence changes associated with fast and slow reactions).

Figure 2A plots k_{obs1} and k_{obs2} versus [TNP-ATP] for binding reactions measured at pH 7.4 and pH 6. At pH 7.4, both fast and slow rate constants increase monotonically with [TNP-ATP]. Rate-constants obtained at 500 μM TNP-ATP show somewhat greater standard errors about the mean. This most likely results from significantly increased TNP-ATP fluorescence self-quenching at this concentration. This attenuates the measured fluorescence change and reduces the sample signal-to-noise ratio. Regression analysis of the [TNP-ATP] dependence of k_{obs1} and k_{obs2} at pH 7.4 indicates that regression fits (slopes and predicted mean k_{obs}) are not

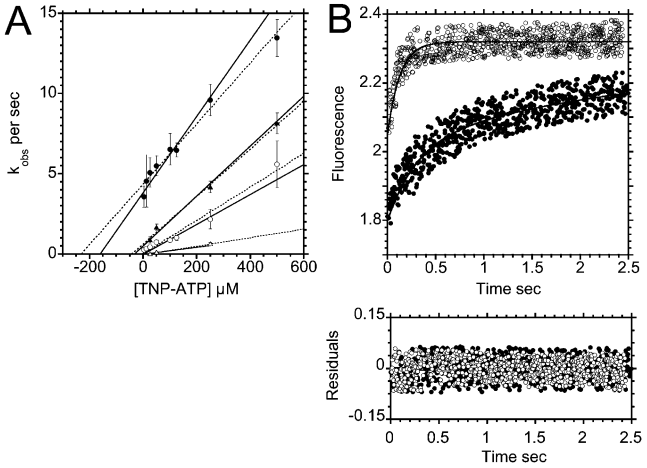

FIGURE 2: (A) TNP-ATP concentration dependence of the time course of TNP-ATP binding to GluT1. Time course data were collected as in Figure 1A. Data were collected at 1 ms intervals, and results from at least four separate runs were averaged then subjected to two exponent analysis (eq 2) by non linear regression. Fast (k_{obs1}) and slow (k_{obs2}) rate constants were averaged from four separate experiments and plotted at mean ± SEM. Ordinate: [TNP-ATP] in μM. Abscissa: rate constant, k_{obs} for increased TNP-ATP fluorescence. Data were collected at pH 7.4 (●, ○) or at pH 6 (▲, △). Results are shown for fast (●, ▲) and slow (○, △) rate constants. The dashed straight lines drawn through the points were computed by linear regression and have the following constants: pH 7.4, fast reaction (●), k_{-1} (y-intercept) = 4.36 ± 0.22 s^{-1}, k_1 (slope) = 18.9 ± 1.0 × 10^3 M^{-1} s^{-1}, R^2 = 0.982; slow reaction (○), k_{-1} (y-intercept) = 0.049 ± 0.049 s^{-1}, k_1 (slope) = 10.4 ± 0.7 × 10^3 M^{-1} s^{-1}, R^2 = 0.972; pH 6.0, fast reaction (▲), k_{-1} (y-intercept) = 0.674 ± 0.197 s^{-1}, k_1 (slope) = 14.8 ± 0.7 × 10^3 M^{-1} s^{-1}, R^2 = 0.996; slow reaction (△), k_{-1} (y-intercept) = 0.032 ± 0.007 s^{-1}, k_1 (slope) = 0.198 ± 0.037 × 10^3 M^{-1} s^{-1}, R^2 = 0.959. Regression analysis of pH 7.4 data omitting the 500 μM TNP-ATP data points resulted in the following constants: fast reaction (●), k_{-1} (y-intercept) = 4.19 ± 0.22 s^{-1}, k_1 (slope) = 21.8 ± 1.9 × 10^3 M^{-1} s^{-1}, R^2 = 0.964; slow reaction (○), k_{-1} (y-intercept) = 0.249 ± 0.061 s^{-1}, k_1 (slope) = 7.4 ± 0.5 × 10^3 M^{-1} s^{-1}, R^2 = 0.975. Comparison of regression fits of pH 7.4 experimental data lacking or containing the 500 μM TNP-ATP data points shows that neither the computed slopes nor the average predicted k_{obs} are significantly different (two-tailed t-test, $p < 0.05$). The solid straight lines drawn through the points were computed by simulating the time course of binding using Scheme 1, followed by deconvolution of the simulated time courses into fast and slow components. The following constants produced the best fits to the experimental data: pH 7.4, K_N = 530 μM, k_1 = 6 × 10^3 M^{-1} s^{-1}, a = 0.2, b = 0.01, c = 0.001; pH 6, K_N = 120 μM, k_1 = 4.4 × 10^3 M^{-1} s^{-1}, a = 0.2, b = 0.01, c = 0.001. (B) Time course of TNP-ATP binding to GluT1 at pH 6 at 250 μM TNP-ATP (●) and at 500 μM TNP-ATP (○). Data were collected at 1 ms intervals, and results from at least four separate runs were averaged then subjected to one- or two exponent analysis (eqs 1 and 2) by non linear regression. 500 μM TNP-ATP data were fitted equally well by one and two exponents (in the latter instance, nonlinear regression converged to produce two identical rate constants). The line drawn through the points has the following constants: C = 2.05 ± 0.04%, k_1 = 7.92 ± 0.59 s^{-1}, ΔE = 0.27 ± 0.04%, R^2 = 0.79. 250 μM TNP-ATP data were fitted best by 2-exponents. The line drawn through the points has the following constants two exponentials, C = 1.81 ± 0.07%, k_1 = 3.42 ± 0.19 s^{-1}, ΔE_1 = 0.221 ± 0.007%, k_2 = 0.376 ± 0.25 s^{-1}, ΔE_2 = 0.25 ± 0.03%, R^2 = 0.83. The data below the plot shows the residuals of these fits.

significantly different if k_{obs} obtained at 500 μM TNP-ATP are omitted (see Figure 2 legend).

This behavior is consistent with the hypothesis that fast and slow components represent second-order reactions of the form

$$\text{GluT1} + \text{TNP-ATP} \underset{k_{-1}}{\overset{k_1}{\rightleftharpoons}} \text{GluT1.TNP-ATP}$$

Thus, for both fast and slow reactions, the pseudo-first-order rate constant for TNP-ATP binding, k_{obs}, is $k_{-1} + k_1$ [TNP-ATP]. The data of Figure 2A may be used to calculate k_1 and k_{-1} for fast and slow reactions as the slope and y-intercept respectively of linear fits of k_{obs} versus [TNP-ATP]. At pH 7.4, the fast reaction is resolved as k_1 = 1.89 × 10^4 M^{-1} s^{-1} and k_{-1} = 4.4 s^{-1}. $K_{d(app)}$ for the reaction (k_{-1}/k_1) is 233 μM. The second (slow) component of binding at pH 7.4 is resolved as k_1 = 1.0 × 10^4 M^{-1} s^{-1} and k_{-1} = 0.15 s^{-1} with $K_{d(app)}$ = 15 μM.

Our previous studies (*11*) (and see here) demonstrate that reduced pH enhances azidoATP binding to GluT1. Figure 2A also shows the concentration dependence of TNP-ATP binding to GluT1 at pH 6.0. The rapid, low-affinity component of binding observed at pH 7.4 is absent at pH 6. The slow (high affinity) component of binding persists at pH 6 and a slower, high-affinity component of binding is also revealed. This latter component disappears at higher [TNP-ATP], where time-course data follow monoexponential kinetics (Figure 2B). These data are consistent with the hypothesis that reduced pH converts low-affinity TNP-ATP binding to high-affinity binding by reducing TNP-ATP dissociation from the TNP-ATP·GluT1 complex (y-intercepts (k_{-1}) are reduced at low pH; Figure 2A).

Figure 3A summarizes the effects of ATP and AMP on the time course of TNP-ATP (100 μM) binding to GluT1. Both nucleotides enhance the rate of TNP-ATP interaction with GluT1 (fast and slow components of binding are accelerated). With ATP, fast and slow binding components increase in a saturable fashion with [ATP]. This action of ATP is half-maximal at 40−80 μM ATP (see Figure 3A) and results in a 5−7-fold increase in the rate of TNP binding to GluT1. Low concentrations of AMP (50−500 μM) also enhance the rate of TNP-ATP interaction with GluT1. This effect is almost completely lost at 2 mM AMP (Figure 3A). ATP enhances the magnitude of the fast first-order fluorescence change upon TNP-ATP binding but reduces the extent of the slow reaction (Figure 3B). AMP reduces the magnitude of both fast and slow first-order fluorescence changes promoted upon TNP-ATP interaction with GluT1. Reductions in the extent of fluorescence increase may result from competition of nucleotides with TNP-ATP for binding to GluT1.

Figure 4A shows that the sugar exit site ligand CCB enhances the rate of TNP-ATP binding to GluT1. This is consistent with earlier studies demonstrating that CCB and ATP binding to GluT1 are synergisitic (*25*). Pretreatment of tetrameric GLUT1 with dithiothreitol (2 mM for 20 min) causes transporter dissociation into dimeric GluT1 (*6*) and prevents TNP-ATP interaction with GluT1 (Figure 4B).

GluT1 Photolabeling with AzidoATP. Our previous studies have established that isolated human red blood cell GluT1 is not an ATPase and may be photolabeled at low (4%) efficiency using [γ-^{32}P]-azidoATP in an ATP-protectable fashion (*8*). In the present study, we asked whether prior GluT1 photoirradiation with unlabeled azidoATP protects GluT1 against subsequent photoincorporation of [γ-^{32}P]-azidoATP. To our surprise, the opposite result is obtained. GluT1 (1 μg/μL) was first photoirradiated in the presence

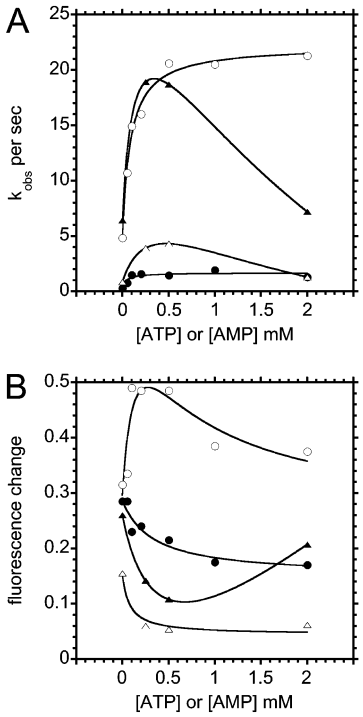

FIGURE 3: (A) Effects of ATP and AMP on TNP-ATP binding to GluT1. Ordinate: [TNP-ATP] in μM. Abscissa: rate constant, k_{obs} for increased TNP-ATP fluorescence. All data were collected at pH 7.4 using 100 μM TNP-ATP. At least four runs were averaged at each competing [nucleotide], and the increase in TNP-ATP fluorescence was resolved as two exponentials characterized by fast and slow rate constants with corresponding fluorescence changes (ΔE_{fast} and ΔE_{slow}). The experiment was repeated at least three times, and results are shown as mean ± SEM. Results are shown for fast (○, ▲) and slow (●, △) rate constants. Results were obtained using ATP (●, ○) or AMP (▲, △) as the competing nucleotide. With ATP, rate constants increase in a saturable manner with [nucleotide], and curves drawn through the points were computed by nonlinear regression, assuming that k_{obs} is described by $k_{obs} = k_o + k_{max}$ [nucleotide]/($K_{0.5}$ + [nucleotide]) where k_o and k_{max} represent k_{obs} for TNP-ATP binding in the absence or presence of saturating nucleotide and $K_{0.5}$ is that [nucleotide] producing $k_{obs} = k_o + 0.5\ k_{max}$. The results are as follows: ATP, fast reaction $k_o = 4.73 \pm 0.82\ s^{-1}$, $k_{max} = 17.46 \pm 0.98\ s^{-1}$, $K_{0.5} = 86.7 \pm 16.9\ \mu$M; ATP, slow reaction $k_o = 0.24 \pm 0.19\ s^{-1}$, $k_{max} = 1.42 \pm 0.35\ s^{-1}$, $K_{0.5} = 41.3 \pm 26.8\ \mu$M. With AMP, rate constants increase then decrease with [nucleotide]. Insufficient data points exist to describe the results in a quantitative manner. The curves were drawn through the points by eye and have no theoretical significance. (B) Effects of AMP and ATP on the extent of TNP-ATP fluorescence change upon interaction with GluT1. The fluorescence changes (ΔE_{fast} and ΔE_{slow}) calculated in 2B are plotted as a function of [ATP] (●, ○) or [AMP] (▲, □). The curves drawn through the points were drawn by eye and have no theoretical significance.

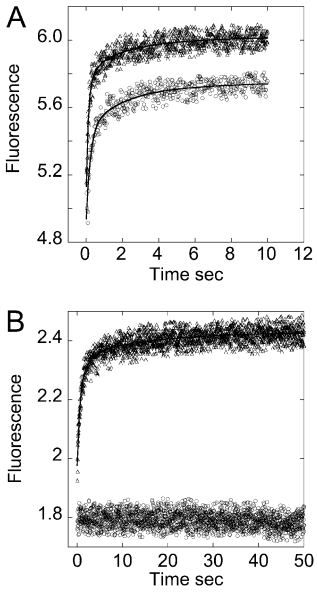

FIGURE 4: Effects of CCB and DTT on TNP-ATP binding to GluT1. (A) Effect of 500 nM CCB and on 100 μM TNP-ATP binding to GluT1 (10 μg). GluT1 was preincubated with 500 nM CCB (○) or saline (□) then mixed with 100 μM TNP-ATP ± 500 nM CCB. Five runs were averaged for each condition. CCB accelerates TNP-ATP binding. The curves drawn through the points were computed by nonlinear regression according to Scheme 1 and have the following constants: control, $K_N = 124\ \mu$M, $k_1 = 15.7 \times 10^3\ M^{-1}\ s^{-1}$, $a = 0.54$, $b = 0.32$, $c = 0.02$; CCB, $K_N = 89\ \mu$M, $k_1 = 17.7 \times 10^3\ M^{-1}\ s^{-1}$, $a = 1.1$, $b = 0.03$, $c = 0.03$. (B) Effect of preincubation with 2 mM DTT on 100 μM TNP-ATP binding to GluT1 (10 μg). GluT1 was preincubated with (○) or without (□) 2 mM DTT for 30 min, sedimented at 14 000*g*, washed once in 100 volumes DTT-free medium, and mixed rapidly with 100 μM TNP-ATP. Five runs were averaged, and the curves drawn through the control points were computed by nonlinear regression according to Scheme 1 and have the following constants: $K_N = 88.6\ \mu$M, $k_1 = 6.2 \times 10^3\ M^{-1}\ s^{-1}$, $a = 0.67$, $b = 0.\ 19$, $c = 0.02$. No TNP-ATP/GluT1 mixing induced increase in fluorescence was observed when GluT1 was first treated with DTT.

or absence of 5 mM unlabeled azidoATP. Irradiated proteoliposomes were sedimented, washed several times in azidoATP-free medium then resuspended in medium containing 5.5 μM [γ-^{32}P]-azidoATP. Ultraviolet irradiation of GluT1 in the presence of unlabeled azidoATP consistently enhances (relative to irradiation in the absence of unlabeled azidoATP) subsequent photoincorporation of [γ-^{32}P]-azidoATP by 2−3-fold (Figure 5). This study also confirms earlier studies (*11*) demonstrating that GluT1 photolabeling by azidoATP is enhanced at pH 5.5 relative to labeling at pH 8.

Effects of Acidification on ATP-Modulation of 3MG Transport. Previous studies from this laboratory have demonstrated that intracellular acidification modifies GluT1 sensitivity to regulation by ATP (*11*). At pH 7.4, the affinity of the red cell sugar transporter for 3MG increases in a saturable manner with [ATP]. At pH 6, low concentrations of ATP (<200 μM) increase the affinity of GluT1 for 3MG and thus stimulate uptake of 100 μM 3MG. Higher, physiological concentrations of ATP (2 mM) fail to stimulate 100 μM 3MG uptake at pH 6. Several questions arise from these observations. (1) Does reduced pH promote GluT1 interaction with cellular factors that negate GluT1 regulation by ATP? (2) Does reduced pH cause a general inhibition of GluT1 mediated sugar transport?

The potential involvement of cellular factors in pH-sensitive sugar transport regulation was investigated by reconstitution of GluT1 into proteoliposomes containing or lacking 4 mM Mg.ATP at pH 7.4 or pH 6. Table 1 shows that 3MG uptake at subsaturating (100 μM) 3MG is accelerated by ATP at pH 7.4. ATP binding to GluT1 is increased at pH 6 (see Figures 2 and 4 and ref *11*), but the effect of ATP on net 3MG uptake is lost (Table 1). Infinite-cis net 3MG uptake (the time course of saturated 3MG uptake) by GluT1 proteoliposomes is also inhibited by ATP at pH 7.4 but is unaffected by ATP at pH 6 (Figure 6). Net

Conditioning								
uv irradiation	-	-	+	+	+	+	+	+
[γ-^{31}P]azidoATP pH 8	-	-	-	-	+	+	-	-
[γ-^{31}P]azidoATP pH 5.5	-	-	-	-	-	-	+	+
Labeling								
uv irradiation	+	+	+	+	+	+	+	+
[γ-^{32}P]azidoATP pH 8	+	-	+	-	+	-	+	-
[γ-^{32}P]azidoATP pH 5.5	-	+	-	+	-	+	-	+

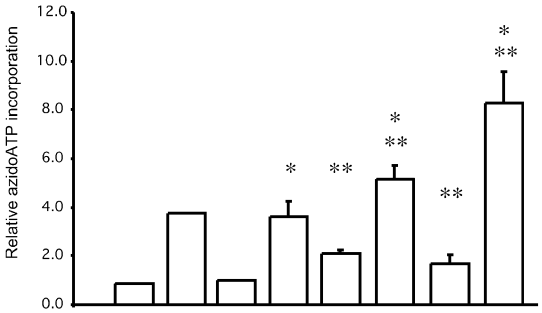

FIGURE 5: Effects of GluT1 UV-cross-linking GluT1 with unlabeled azidoATP on subsequent GluT1 UV cross-linking with [γ-^{32}P]-azidoATP at pH 8 or 5.5. During conditioning, GluT1 (1 μg/μL) was exposed to saline containing or lacking 5 mM unlabeled azidoATP at pH 8 or pH 5.5. The proteoliposomes were UV irradiated on ice for 90 s (two control samples at pH 8 and 5.5 were not UV irradiated), collected by sedimentation at 14 000*g* for 10 min, and washed twice in azidoATP-free medium. Subsequently, during labeling, membranes were exposed to 5.5 μM [γ-^{32}P]-azidoATP at pH 8 or pH 5.5 and UV irradiated on ice for 90 s. Following washing in label-free saline, proteins were resolved by SDS-PAGE, electrophoretically transferred to immobilon membranes, and exposed to film. The intensity of GluT1 [γ-^{32}P]-azidoATP photoincorporation was quantitated by densitometry. The membrane was then subjected to [GluT1] quantitation by immunoblot analysis using C-Ab, and [γ-^{32}P]-azidoATP photoincorporation was normalized for the amount of immunodetectable GluT1 in each lane. This experiment was repeated three times. Ordinate: relative [γ-^{32}P]-azidoATP photoincorporation. Results are shown as mean ± SEM. There is no significant difference in [γ-^{32}P]-azidoATP labeling when samples are conditioned (in the absence of azidoATP) with or without UV exposure. *Indicates that [γ-^{32}P]-azidoATP photoincorporation at pH 5.5 is significantly greater than label incorporation at pH 8.0 ($p < 0.005$). **Indicates that [γ-^{32}P]-azidoATP photoincorporation is significantly greater ($p < 0.005$) following conditioning by UV-irradiation in the presence of unlabeled azidoATP (5 mM) than it is following conditioning by UV-irradiation in the absence of azidoATP.

transport inhibition by ATP appears to result from (1) increased transporter affinity for 3MG (efflux saturates at lower [3MG]) and (2) reduced V_{max} for net transport (Table 1). These results demonstrate that pH modulation of ATP regulation of GluT1-mediated sugar transport is recapitulated in an in vitro reconstituted system.

We compared the fundamental characteristics of carrier-mediated 3MG transport at pH 6 and 7.4 by analysis of zero-trans and infinite-trans unidirectional 3MG uptake in resealed human red cell ghosts containing or lacking 4 mM ATP. Table 2 shows that the presence of 50 mM intracellular 3MG results in accelerated unidirectional 3MG uptake at both acidic and normal pH. ATP modulates zero-trans fluxes only at pH 7.4. The effects of ATP on exchange transport at pH 7.4 and pH 6 are not significant at the $p < 0.05$ level (Table 2).

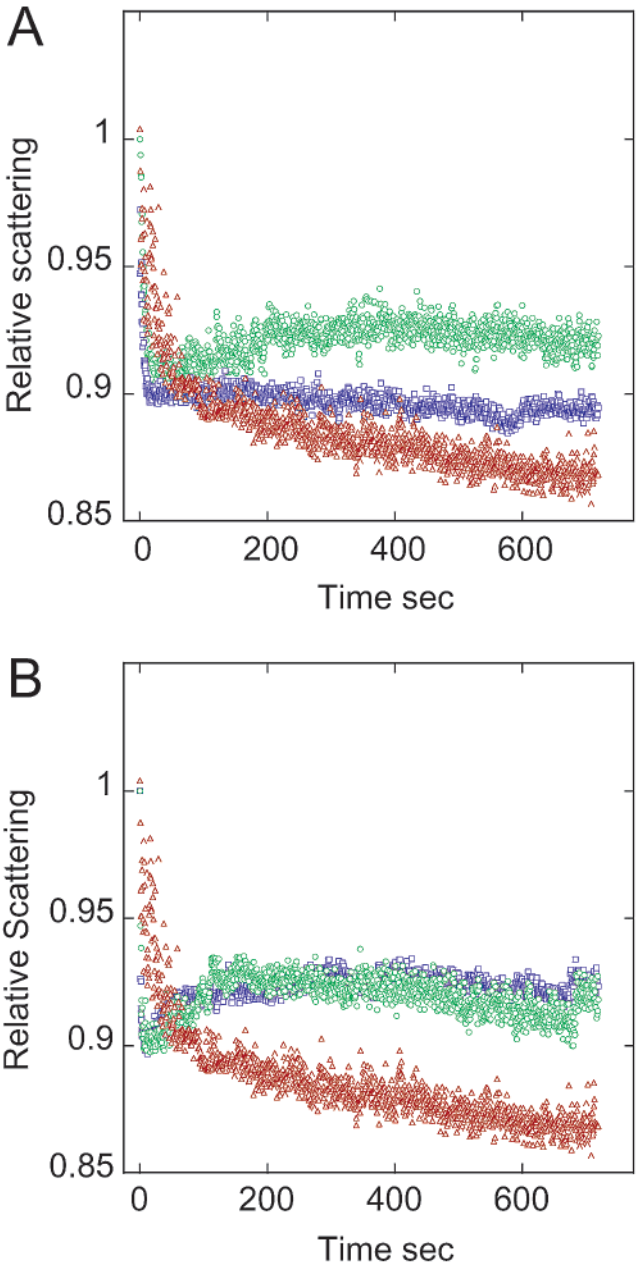

FIGURE 6: Effects of pH on GluT1-mediated infinite-cis net sugar uptake by reconstituted GluT1-proteoliposomes. Results are shown for transport at pH 7.4 (A) and at pH 6 (B). GluT1 proteoliposomes were prepared as described in materials and methods and were injected into saline containing 120 mM sucrose (□), 120 mM 3MG (○), or 120 mM 3MG plus 2 mM Mg.ATP (□). Proteoliposomes injected into ATP-containing medium also contained 2 mM Mg.ATP in the intraliposomal space. Light scattering at 450 nm was averaged over 0.5 s intervals and plotted as a function of time. Each data set represents the average of three or more separate runs. Proteoliposomes first shrink due to osmotic water loss and then swell as 3MG is transported into the intraliposomal space and water follows.

DISCUSSION

The present study was formulated to answer two questions. (1) Is ATP binding to the glucose transporter a simple or cooperative process? (2) How does the ATP-liganded state of the glucose transporter influence transporter catalytic efficiency? Our findings suggest a working hypothesis for nucleotide-dependent, allosteric regulation of GluT1-mediated sugar transport. This model may also explain why some

Table 1: Effect of pH on ATP Modulation of Reconstituted GluT1-Mediated 3MG Transport

pH[a]	6	6	7.4	7.4
[ATP][b] (mM)	0	2	0	2
unidirectional 100 μM 3MG uptake[c]	125.8 ± 4.0[d]	131.2 ± 5	105.9 ± 10.8	238.8 ± 17.8
π[e]	8.39×10^{-4}	8.73×10^{-4}	7.07×10^{-4}	1.59×10^{-3}
infinite-cis net 3MG uptake[f]				
K^{zt}	1.67 ± 0.31	1.47 ± 0.16	1.61 ± 0.05	0.31 ± 0.04
K^{ic}	1.79 ± 0.69	2.23 ± 0.20	2.1 ± 0.09	1.28 ± 0.06
V^{zt}	0.53 ± 0.010	0.49 ± 0.07	0.47 ± 0.03	0.16 ± 0.03
V^{ee}	0.98 ± 0.19	1.43 ± 0.25	0.91 ± 0.10	1.23 ± 0.22
π_{3MG}[g]	0.32 ± 0.09	0.33 ± 0.05	0.29 ± 0.02	0.51 ± 0.07
Pf_{nt}[h]	39 ± 17	46 ± 13	100 ± 37	56 ± 18
Pf_t[h]	113 ± 39	87 ± 33	164 ± 11.3	103 ± 24.3

[a] Uptake of 3MG was measured in GluT1 proteoliposomes reconstituted in and maintained in saline at pH 6 or 7.4. [b] Proteoliposomes contained either 0 or 2 mM Mg.ATP and were resuspended in saline containing or lacking ATP. [c] Unidirectional 100 μM 3MG uptake was measured at 4 °C. Uptake is measured as μmol/L proteolioposome water/min. [d] Results are shown as mean ± SEM, with $n = 3$. [e] π is the ratio uptake rate/[3MG] and has units of μm/s. This is formally equivalent to $V_{max}/K_{m(app)}$ and is also the 3MG permeability coefficient of the membrane. Human RBCs are characterized by $\pi_{3MG} = 1.2 \times 10^{-3}$ μM/s at 4 °C (*20*). [f] Infinite-cis net uptake of 3MG (the time course of 120 mM 3MG uptake by sugar-free proteoliposomes at 20 °C). Time courses of transport (three or more runs were averaged for each condition) were analyzed to obtain the parameters R_{oo}, R, R_{ee}, and K as described in Materials and Methods. K^{zt} (K_m for net uptake), V^{zt} (V_{max} for net uptake), K^{ic} (that concentration of intraliposomal 3MG that reduces net sugar uptake by 50%), and V^{ee} (V_{max} for exchange transport) were calculated as KR_{oo}/R, $1/R$, KR/R_{ee}, and $1/R_{ee}$ respectively. K parameters have units of mM. V_{max} parameters have units of nmol/cm^2 surface area/s. [g] π_{3MG} (μM/s) for infinite-cis net uptake was computed as $V^{zt}/K^{zt} = 1/KR_{oo}$. Human RBCs are characterized by $\pi_{3MG} = 0.26$ μM/s at 20 °C (*20*). [h] The hydraulic water permeability coefficients of GluT1-free (Pf_{nt}) and GluT1-containing (Pf_t) liposomes (units cm/s).

Table 2: Effects of Altered pH on Net and Exchange 3MG Transport in Red Cell Ghosts[a]

	3MG uptake[b]			
pH	control[c]	ATP[d]	3MG[e]	ATP + 3MG[f]
7.4	10.7 ± 1.1	17.4 ± 1.7	39.2 ± 5.4	38.9 ± 7.3
P (control vs test)[g]		0.0030	0.0039	0.0062
P (3MG vs 3MG + ATP)[h]				0.9865
6	11.3 ± 1.9	12.4 ± 0.7	39.6 ± 4.2	26.1 ± 3.6
P (control vs test)[g]		0.3278	0.0023	0.0164
P (3MG vs 3MG + ATP)[h]				0.0149
P (pH 7.4 vs 6)[i]	0.8186	0.0884	0.9480	0.1980

[a] Uptake of 100 μM 3MG at 4 °C was measured under zero-trans (Control and ATP) and exchange (3MG and 3MG + ATP) conditions. [b] Uptake has units of μmol of 3MG transported per L cell water per min and is shown as mean ± SEM of five separate paired experiments made in triplicate. Red cell ghosts were hypotonically lyzed at 4 °C in pH 7.4 lysis buffer and then were resealed at pH 7.4 or at pH 6 in KCl medium lacking [c] or containing 4 mM Mg.ATP,[d] 50 mM 3MG,[e] or 4 mM Mg.ATP + 50 mM 3MG.[f] [g] Probability that this test result is identical to control at the same pH (one-tailed students *t*-test). [h] Probability that exchange transport + ATP is identical to exchange transport without ATP at the same pH (two-tailed students *t*-test). [i] Probability that the result at pH 6 is identical to the same test condition at pH 7.4 (two-tailed students *t*-test).

cells respond acutely to cellular metabolic depletion with accelerated GluT1-mediated sugar transport while sugar transport in other GluT1-expressing cells is insensitive to metabolic stress.

Previous in vitro and in vivo studies from this laboratory have established that the human red blood cell glucose transport protein is an adenine nucleotide binding protein (*8*). GluT1 lacks intrinsic ATPase capacity but, when complexed with ATP, responds with reduced V_{max} and $K_{m(app)}$ for net sugar uptake and with increased $K_{m(app)}$ and reduced V_{max} for net sugar exit (*7*). Exchange sugar transport capacity (sugar uptake coupled to sugar exit) is unaffected by ATP (*9*). AMP and ADP also interact with isolated GluT1 and, when restored to the interior of red cell ghosts, antagonize the action of ATP on net sugar transport (*11*). ATP appears to inhibit net sugar transport by promoting a carrier conformational change that occludes newly imported sugars within a cage or vestibule formed by GluT1 cytosolic domains (*10*). In the presence of ATP, diffusion of sugar from the occlusion cage to cytosol or from cytosol to occlusion cage is severely limited. For a newly imported sugar molecule entering the occlusion cage, the probability of recycling to the interstitium via sugar export is thus greater than the likelihood of release into cytosol. Net sugar exit is depressed because the catalytic (exit) site is accessible only to only those sugar molecules within the cage and diffusion from cytosol to occlusion cage is limiting. When ATP levels fall, it is hypothesized that the internal cage opens permitting less restricted exchange of sugars between the catalytic (exit) site and cytosolic water. It is uncertain at this time whether substrate occlusion per se accounts for sugar transport control by ATP or whether GluT1-mediated sugar translocation from interstitium to occlusion cage and vice versa are also affected by ATP binding to GluT1.

Several indirect lines of evidence suggest that ATP binding to the glucose transport protein is a cooperative process. Transporter exposure to reductant promotes dissociation of normally tetrameric GluT1 into dimeric GluT1 (*5*, *25*). Unlike tetrameric GluT1, dimeric GluT1 is a poor target for photolabeling by [γ-^{32}P]azidoATP (*11*) and, as shown here, fails to bind TNP-ATP. Exposure of tetrameric GluT1 to acidic medium (pH 6−5.5) increases [γ-^{32}P]azidoATP photolabeling of GluT1 by as much as 11-fold relative to photolabeling at pH 8.0 (*11*). ATP and CCB binding to tetrameric GluT1 are synergistic (*25*). These findings suggest that ATP interacts with pH-sensitive GluT1 domains exposed only in the GluT1 homotetramer.

Studies examining the concentration dependence of nucleotide modulation of GluT1 function have not produced evidence for cooperative nucleotide binding. ELISA of ATP modulation of GluT1-carboxyl-terminal peptide antibody binding to GluT1 suggests that ATP binding to GluT1 is a simple, high affinity, saturable process (*8*). Inhibition of [γ-^{32}P]azidoATP photolabeling of GluT1 by ATP, ADP, or by AMP appears to be a simple competitive phenomenon (*8*, *11*). ATP modulation of sugar transport in resealed human red cell ghosts and in inside-out-vesicles is characterized by a simple saturable dependence on [ATP] with half-maximal effects at approximately 150−600 μM (*11*, *26*). Nucleotide-induced quenching of GluT1-intrinsic tryptophan fluorescence reveals some evidence for cooperativity in nucleotide binding (*26*). However, none of these studies is conclusive. Tryptophan fluorescence quenching studies are complicated by low signal-to-noise at low nucleotide concentrations (where cooperativity is most marked) and by increasing nonspecific (inner filter) effects at higher nucleotide levels. Transport measurements made using red cell ghosts and inside-out-vesicles require multiple determinations at each nucleotide concentration employed, thus limiting the range of nucleotide concentrations tested in practice. Intracellular nucleotide hydrolysis by cytosolic ATPases and nucleotide phosphorylation by adenylate kinase further complicates interpretation of studies with ghosts (*14*). Studies with isolated GluT1 examining nucleotide inhibition of [γ-^{32}P]-azidoATP photolabeling and nucleotide modulation of C-Ab binding have also employed a limited range of nucleotide concentrations and additionally suffer from a low signal-to-noise at low [nucleotide].

The present study examines nucleotide binding to GluT1 by analysis of the increase in fluorescence of TNP-ATP brought about upon binding to GluT1. Free trinitrophenyl (TNP) nucleotides are nonfluorescent in water but undergo an equilibrium transition to a semiquinoid structure characterized by relatively long-wavelength spectral properties (*27*). This form is fluorescent when bound to the nucleotide-binding site of some proteins. (*27*). Signal-to-noise problems at low ligand concentrations are significantly improved by this approach, for while nucleotide binding is low at subsaturating nucleotide concentrations, background fluorescence is also low. Contrast this situation with nucleotide-induced GluT1 intrinsic tryptophan fluorescence quenching, where background fluorescence is high in the absence of nucleotide and where total fluorescence quenching may be as low as 3 to 5% at saturating [nucleotide] (*26*).

Rapid mixing of GluT1 and TNP-ATP results in the time-dependent increase in TNP-ATP fluorescence. This increase is unrelated to trans-bilayer diffusion of TNP, to delays in equilibration of the interior of leaky proteoliposomes with extraliposomal TNP-ATP, or to interaction with the hydrophobic lipid bilayer (see Results). The time course of TNP-ATP binding to GluT1 proteoliposomes can be resolved as the sum of at least two (fast and slow) GluT1-dependent exponential processes. This behavior is not explained by the use experimental conditions (e.g., [GluT1] $\sim$ [TNP-ATP]) that require the use of second-order rate analysis because the even the lowest [TNP-ATP] employed is more than 13-fold greater than [GluT1]. Rather, these results are consistent with a more complex binding reaction (multiple processes in series or in parallel). Analysis of the TNP-ATP concentration dependence of binding assuming two components of binding demonstrates that both fast and slow components of binding are accelerated with increasing [TNP-ATP]. The fast component of binding increases linearly with [TNP-ATP], indicating a second-order reaction with association (k_1) and dissociation (k_{-1}) rate constants of 19×10^3 M^{-1} s^{-1} and 4.4 s^{-1}, respectively, and $K_{d(app)} = k_{-1}/k_1 = 232$ μM. The slower component of binding is consistent with k_1 and k_{-1} of 10×10^3 M^{-1} s^{-1} and 0.15 s^{-1}, respectively, and $K_{d(app)} = k_{-1}/k_1 = 15$ μM.

Several observations lead us to conclude that these binding reactions are dependent and GluT1-mediated. Isolated human red cell GluT1 is comprised of 90% GluT1. The two major contaminants are band 7 protein and nucleoside transporter (*28*). Band 7 protein is not labeled by [γ-^{32}P]azidoATP (*8*), while specific extraction of labeled GluT1 by immunoprecipitation using anti-GluT1 carboxyl terminal peptide-directed antibodies results in quantitative depletion of photolabeled protein (*8*). GluT1 photolabeling, therefore, accounts quantitatively for [γ-^{32}P]azidoATP photoincorporation into proteins present in GluT1 proteoliposomes. This conclusion is strengthened by the finding that prior treatment of GluT1 with DTT quantitatively inhibits azidoATP labeling of GluT1 and prevents increased TNP-ATP fluorescence upon mixing GluT1 and TNP-ATP. These observations support the conclusion that the ATP binding component of GluT1 proteoliposomes is the DTT-sensitive GluT1 homotetramer.

The observable, second-order rate constant, $k_{1(app)}$ for TNP-ATP binding is proportional to the intrinsic association rate-constant for TNP-ATP interaction with GluT1(k_1) and the concentration of available ATP binding sites ([GluT1] $\div$ n, where n is the number of GluT1 molecules required to form an ATP binding site). The ratio of $k_{1(app)}$ for fast and slow reactions in the present study is 2:1, suggesting, if the intrinsic association constants for fast and slow reactions are similar, that the slow binding sites account for as much as 33% of the total population of available sites. Since binding to GluT1 quantitatively accounts for nucleotide binding to the GluT1 preparation (see above), this suggests that either (1) fast (low affinity) and slow (high affinity) interactions of TNP-ATP with GluT1 (but not other species) occur in parallel or (2) fast and slow reactions occur in series and are manifest as cooperative TNP-ATP binding to GluT1. The latter hypothesis seems more probable for two reasons. (1) Biphasic binding kinetics are lost with increasing nucleotide concentration at pH 6. (2) Intracellular ATP modulates 3MG transport in human red blood cell ghosts at acidic intracellular pH in a biphasic manner (*11*). Transport is stimulated at ATP

= 200 μM but is inhibited at higher [ATP]. Importantly, this effect cannot be modeled simply as the sum of ATP inhibition of one population of transporter plus ATP stimulation of a second GluT1 population (*11*).

Further evidence for cooperative nucleotide binding is available from studies in which progressive addition of ATP or AMP increases the rate at which TNP-ATP interacts with GluT1 while reducing the number of available sites for interaction with TNP-ATP. Moreover, enhancement of [γ-^{32}P]azidoATP photolabeling of GluT1 by prior irradiation in the presence of saturating unlabeled azidoATP suggests that low-efficiency, covalent attachment of unlabeled ligand to one or more nucleotide binding sites within a carrier complex increases the efficiency of labeling of remaining sites for [γ-^{32}P]azidoATP.

We have modeled TNP-ATP binding to the glucose transporter as a cooperative process in which each GluT1 protein of the tetramer presents a single nucleotide binding domain. At this time there are insufficient data to indicate whether the nucleotide binding site:GluT1 molar ratio is 1:1 or lower. Estimates of ethenoATP binding to GluT1 suggest 1 mol nucleotide binding sites per mol CCB binding sites (*8*). However, since nonreduced GluT1 exposes only 1 mol CCB binding sites per 2 mol GluT1 (*5*), tetrameric GluT1 may normally present only two nucleotide binding sites per transporter complex. The results of the present study are best modeled by the Adair−Pauling sequential interaction model when three or more nucleotide binding sites per carrier complex are assumed (see Scheme 1). Thus, a critical test of this hypothesis will be the accurate determination of GluT1 nucleotide binding capacity. Assuming four nucleotide binding sites per carrier complex and that all nucleotide binding sites in the unliganded carrier adopt the low-affinity state, binding of the first nucleotide to the tetramer enhances TNP-ATP binding to the remaining nucleotide binding sites by reducing K_d (specifically by reducing k_{-1}) for binding by 5-fold. Progressive occupancy of available sites by TNP-ATP increasingly augments the affinity of the remaining site-(s) for TNP-ATP by 10-fold per nucleotide addition. This model is compatible with the TNP-ATP binding data of Figures 1 and 2.

pH-sensitive ATP binding may result from protonation of side chains within the ATP binding domain. Histidine is the obvious candidate amino acid for side-chain protonation, as pH is lowered from 8.5 to 5.5 and GluT1 contains five histidine residues, of which four (H 160, 239, 337, and 484) are located within cytoplasmic domains. Exofacial His_{50} is a poor candidate since red cell sugar transport is insensitive to altered extracellular pH (*29*). His_{337} lies within the intracellular portion of the GluT1 ATP binding domain (residues 301−361) identified previously by N-terminal sequence analysis of proteolytic fragments obtained from azidoATP-labeled GluT1 (*11*). Protonation of His_{337} could enhance ATP binding directly by increasing ionic interaction between ATP and His^+ within the binding pocket. Alternatively, protonated His_{337} might now participate in a cation−π interaction (*30*) with, for example, Phe_{326} or could interfere with a cation−π interactions through ionic repulsion of cation-bearing side chains (e.g., Arg_{330}, Arg_{3333}, or Arg_{334}). In the absence of detailed knowledge of the GluT1 ATP binding domain and pH-dependent GluT1 conformational changes, these possibilities remain speculative. However, we address these possibilities specifically by mutagenesis in the accompanying paper (*31*).

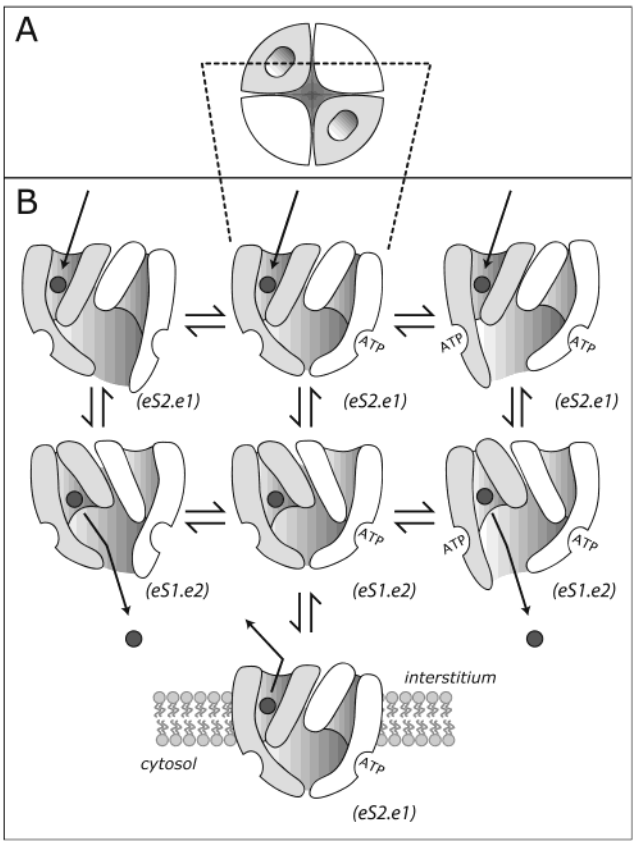

FIGURE 7: Model for pH modulation of ATP-regulation of sugar transport. (A) The glucose transporter (viewed from above the cell membrane) is a complex of four GluT1 proteins (subunits). (B) The transporter is sectioned (normal to the plane of the bilayer) through the catalytic center of two of the four subunits. In the absence of ATP, the cytosolic domains of the transporter present a relaxed conformation through which any newly imported sugar molecule can gain unrestricted access to bulk cytosol. When one ATP is bound per GluT1 dimer, cytosolic domains of the transporter undergo a conformational change, forming a cage around the sugar exit sites which restricts access to bulk cytosol. A newly imported sugar now has a greater probability of being recycled to the interstitium via translocation (eS1.e2 → eS2.e1 conformational change) than release into cytosol. When a second ATP molecule interacts with the transporter, cytosolic domains of the transporter adopt a third conformation in which the cage surrounding the exit site is once more relaxed and sugars can freely access bulk cytosol.

Why is the transporter's catalytic response to ATP lost under conditions (pH 6) where ATP binding to GluT1 is enhanced? We propose that in the absence of bound nucleotide (see Figure 7), the GluT1 cytosolic occlusion cage is relaxed, and intracellular sugars have unrestricted access to the sugar export site. Net sugar uptake, being unrestricted by release from the occlusion cage to cytosol, is characterized by high throughput, low-affinity kinetics. When two ATP molecules are bound to the carrier, ATP-dependent conformational changes close the occlusion cage around the exit site, significantly restricting the release of newly imported sugar into cytosol and thus increasing the likelihood of substrate recycling to interstitium. Although the rate of sugar translocation across the membrane is unchanged, inhibition of release of translocated sugar results in the appearance of high-affinity, low-throughput kinetics (uptake saturates at low extracellular sugar levels). When all four subunits of the

carrier are liganded with ATP, cooperative interactions result in relaxation of the occlusion cage and facilitate the rapid release of imported sugars into the cell water.

We propose that only two ATP binding sites per transporter complex are complexed with ATP at pH 7.4. As pH is lowered to 6, the intrinsic affinity of the nucleotide binding site for ATP is increased by 5-fold, thereby promoting occupation of all four nucleotide binding sites at physiological [ATP]. This model accounts for the effects of reduced pH on GluT1 photolabeling by azidoATP and can explain acidification-induced biphasic ATP-modulation of GluT1 mediated sugar transport. At low pH and low [ATP], the transporter is only partially complexed by ATP and is thus occluded. As ATP levels are raised further, all 4 subunits are occupied by ATP and the occlusion cage relaxes. The model is also consistent with demonstrations of unaltered exchange sugar transport at pH 6. Saturation of the occlusion cage with unlabeled sugars prevents the appearance of ATP-modulation of transport. Unlabeled saturating sugar competes with newly imported labeled sugar for the exit site and thus increases the probability of release of labeled sugar into the cytosol.

This model may also account for variable, cellular sugar transport responses to metabolic challenge. Some GluT1 expressing cells respond to metabolic depletion with rapid acceleration of net sugar transport. This results from either (1) increased catalytic turnover of GluT1 (*4*, *7*, *9*, *14*, *32*−*34*) or (2) increased cell surface GluT1 content (*35*, *36*). However, some GluT1-expressing cells are unresponsive to cellular metabolic stress (*37*, *38*). The present study is most germane to regulation of GluT1 catalytic turnover. A lack of response to altered cellular metabolic status suggests that GluT1 no longer senses cellular metabolic status or, that the effector mechanism is altered. GluT1 in metabolism-insensitive cells may be converted to the high (ATP-binding) affinity disoccluded state or may interact with other cellular factors that relax the occlusion cage.

REFERENCES

1. Zoccoli, M. A., Baldwin, S. A., and Lienhard, G. E. (1978) The monosaccharide transport system of the human erythrocyte. Solubilization and characterization on the basis of cytochalasin B binding, *J. Biol. Chem. 253*, 6923−6930.
2. Kasahara, M., and Hinkle, P. C. (1977) Reconstitution and purification of the D-glucose transporter from human erythrocytes, *J. Biol. Chem. 253*, 7384−7390.
3. Mueckler, M., Caruso, C., Baldwin, S. A., Panico, M., Blench, I., Morris, H. R., Allard, W. J., Lienhard, G. E., and Lodish, H. F. (1985) Sequence and structure of a human glucose transporter, *Science 229*, 941−945.
4. Diamond, D., and Carruthers, A. (1993) Metabolic control of sugar transport by derepression of cell surface glucose transporters: an insulin-independent, recruitment-independent mechanism of regulation, *J. Biol. Chem. 268*, 6437−6444.
5. Hebert, D. N., and Carruthers, A. (1992) Glucose transporter oligomeric structure determines transporter function. Reversible redox-dependent interconversions of tetrameric and dimeric GLUT1, *J. Biol. Chem. 267*, 23829−38.
6. Zottola, R. J., Cloherty, E. K., Coderre, P. E., Hansen, A., Hebert, D. N., and Carruthers, A. (1995) Glucose transporter function is controlled by transporter oligomeric structure. A single, intramolecular disulfide promotes GLUT1 tetramerization, *Biochemistry 34*, 9734−47.
7. Cloherty, E. K., Diamond, D. L., Heard, K. S., and Carruthers, A. (1996) Regulation of GLUT1-mediated sugar transport by an antiport/uniport switch mechanism, *Biochemistry 35*, 13231−13239.
8. Carruthers, A., and Helgerson, A. L. (1989) The human erythrocyte sugar transporter is also a nucleotide binding protein, *Biochemistry 28*, 8337−8346.
9. Helgerson, A. L., Hebert, D. N., Naderi, S., and Carruthers, A. (1989) Characterization of two independent modes of action of ATP on human erythrocyte sugar transport, *Biochemistry 28*, 6410−6417.
10. Heard, K. S., Fidyk, N., and Carruthers, A. (2000) ATP-dependent substrate occlusion by the human erythrocyte sugar transporter, *Biochemistry 39*, 3005−3014.
11. Levine, K. B., Cloherty, E. K., Fidyk, N. J., and Carruthers, A. (1998) Structural and physiologic determinants of human erythrocyte sugar transport regulation by adenosine triphosphate, *Biochemistry 37*, 12221−32.
12. Laemmli, U. K. (1970) *Nature 270*, 680−685.
13. Sultzman, L. A., and Carruthers, A. (1999) Stop-flow analysis of cooperative interactions between GLUT1 sugar import and export sites, *Biochemistry 38*, 6640−50.
14. Hebert, D. N., and Carruthers, A. (1986) Direct evidence for ATP modulation of sugar transport in human erythrocyte ghosts, *J. Biol. Chem. 261*, 10093−10099.
15. Carruthers, A., and Melchior, D. L. (1983) Asymmetric or symmetric? Cytosolic modulation of human erythrocyte hexose transfer, *Biochim. Biophys. Acta 728*, 254−266.
16. Tinoco Jr., I., Sauer, K., and Wang, J. C. (1985) *Physical Chemistry. Priciples and Applications in Biological Sciences*, pp 275−356, Prentice Hall, Englewood Cliffs.
17. Segel, I. H. (1975) *Enzyme Kinetics*, pp 355−385, Wiley, New York.
18. Stein, W. D. (1986) *Transport and Diffusion Across Cell Membranes*, Academic Press, New York.
19. Carruthers, A. (1991) Mechanisms for the facilitated diffusion of substrates across cell membranes, *Biochemistry 30*, 3898−3906.
20. Carruthers, A., and Zottola, R. J. (1996) in *Handbook of Biological Physics. Transport Processes in Eukaryotic and Prokaryotic Organisms*. (Konings, W. N., Kaback, H. R., and Lolkema, J. S., Eds.), pp 311−342, Elsevier, New York.
21. Hiratsuka, T. (1982) Biological activities and spectroscopic properties of chromophoric and fluorescent analogs of adenine nucleoside and nucleotides, 2′,3′-O-(2,4,6-trinitrocyclohexadienylidene) adenosine derivatives, *Biochim. Biophys. Acta 719*, 509−517.
22. Amler, E., Abbott, A., and Ball, W. J. J. (1992) Structural dynamics and oligomeric interactions of Na+,K(+)-ATPase as monitored using fluorescence energy transfer, *Biophys. J. 61*, 553−568.
23. Hunsinger, R. N., and Cheung, H. C. (1986) Probe of the (Ca2+ + Mg2+)-ATPase in erythrocyte membranes of cystic fibrosis patients, *Clin. Chim. Acta 156*, 165−177.
24. Guillen, E., and Hirschberg, C. B. (1995) Transport of adenosine triphosphate into endoplasmic reticulum proteoliposomes, *Biochemistry 34*, 5472−6.
25. Cloherty, E. K., Levine, K. B., and Carruthers, A. (2001) The red blood cell glucose transporter presents multiple, nucleotide sensitive sugar exit sites, *Biochemistry 40*, 15549−15561.
26. Carruthers, A. (1986) Anomalous asymmetric kinetics of human red cell hexose transfer: role of cytosolic adenosine 5′-triphosphate, *Biochemistry 25*, 3592−3602.
27. Hiratsuka, T. (1976) Fluorescence properties of 2′ (or 3′)-O−(2,4,6-trinitrophenyl) adenosine 5′-triphosphate and its use in the study of binding to heavy meromyosin ATPase, *Biochim. Biophys. Acta 453*, 293−7.
28. Baldwin, S. A., Baldwin, J. M., and Lienhard, G. E. (1982) The monosaccharide transporter of the human erythrocyte. Characterization of an improved preparation, *Biochemistry 21*, 3836−3842.
29. Sen, A. K., and Widdas, W. F. (1962) Determination of the temperature and pH dependence of glucose transfer across the human erythrocyte membrane measured by glucose exit, *J. Physiol. 160*, 392−403.
30. Gallivan, J. P., and Dougherty, D. A. (1999) Cation-pi interactions in structural biology., *Proc. Natl. Acad. Sci. U.S.A. 96*, 9459−9464.
31. Levine, K. B., Cloherty, E. K., Hamill, S., and Carruthers, A. (2002) Molecular determinants of sugar transport regulation by ATP, *Biochemistry 41*, 12629−12638.
32. Wood, R. E., and Morgan, H. E. (1969) Regulation of sugar transport in avian erythrocytes, *J. Biol. Chem. 244*, 1451−1460.
33. Carruthers, A. (1986) ATP regulation of the human red cell sugar transporter, *J. Biol. Chem. 261*, 11028−11037.

34. Jung, C. Y., Carlson, L. M., and Whaley, D. A. (1971) Glucose transport carrier activities in extensively washed human red cell ghosts, *Biochim. Biophys. Acta 241*, 613−627.
35. Fischer, Y., Thomas, J., Sevilla, L., Munoz, P., Becker, C., Holman, G., Kozka, I. J., Palacin, M., Testar, X., Kammermeier, H., and Zorzano, A. (1997) Insulin-induced recruitment of glucose transporter 4 (GLUT4) and GLUT1 in isolated rat cardiac myocytes. Evidence of the existence of different intracellular GLUT4 vesicle populations, *J. Biol. Chem. 272*, 7085−92.
36. Sun, D., Nguyen, N., DeGrado, T. R., Schwaiger, M., and Brosius, F. C. r. (1994) Ischemia induces translocation of the insulin-responsive glucose transporter GLUT4 to the plasma membrane of cardiac myocytes, *Circulation 89*, 793−8.
37. Harrison, S. A., Buxton, J. M., and Czech, M. P. (1991) Suppressed intrinsic catalytic activity of GLUT1 glucose transporters in insulin-sensitive 3T3-L1 adipocytes, *Proc. Natl. Acad. Sci. U.S.A. 88*, 7839−43.
38. Harrison, S. A., Buxton, J. M., Helgerson, A. L., MacDonald, R. G., Chlapowski, F. J., Carruthers, A., and Czech, M. P. (1990) Insulin action on activity and cell surface disposition of human HepG2 glucose transporters expressed in Chinese hamster ovary cells, *J. Biol. Chem. 265*, 5793−801.

BI0259002